Photodissociation of Molecular Bromine in Solid H_2 and D_2: Spectroscopy of the Atomic Bromine Spin−Orbit Transition

Sharon C. Kettwich, Leif O. Paulson, Paul L. Raston,† and David T. Anderson*

Department of Chemistry, University of Wyoming, Laramie, Wyoming 82071

Received: April 4, 2008; Revised Manuscript Received: August 22, 2008

We report 355 nm photodissociation studies of molecular bromine (Br_2) trapped in solid parahydrogen (pH_2) and orthodeuterium (oD_2). The product Br atoms are observed via the spin−orbit transition ($^2P_{1/2}$←$^2P_{3/2}$) of atomic bromine. The quantum yield (Φ) for Br atom photoproduction is measured to be 0.29(3) in pH_2 and 0.24(2) in oD_2, demonstrating that both quantum solids have minimal cage effects for Br_2 photodissociation. The effective Br spin−orbit splitting increases when the Br atom is solvated in solid pH_2 (+1.1%) and oD_2 (+1.5%); these increases are interpreted as evidence that the solvation energy of the Br ground fine structure state ($^2P_{3/2}$) is significantly greater than the excited state ($^2P_{1/2}$). Molecular bromine induced H_2 infrared absorptions are detected in the $Q_1(0)$ and $S_1(0)$ regions near 4150 and 4486 cm^{-1}, respectively, which allow the relative Br_2 concentration to be monitored as a function of 355 nm photolysis.

1. Introduction

The photoinitiation of dihalogen dissociation and recombination in cryogenic rare gas (Rg) matrices have long served as prototypical experiments to study the details of molecular photodissociation in a condensed phase.[1−3] The dihalogen has the minimal number of chromophore degrees of freedom, with the dihalogen internuclear distance representing the dissociation coordinate. The Rg atoms form a cage around the dihalogen creating a many-body potential energy barrier to dissociation, and the ability of the Rg atoms to prevent dissociation after photoexcitation is referred to as the cage effect.[4] The structured environment of low-temperature Rg matrices also greatly simplifies the dynamics. The entire dihalogen-Rg matrix condensed-phase system can be assumed to reside in its overall ground state prior to photoexcitation, which means the condensed-phase photoreaction is initiated from a well-characterized nearly pure state. For these reasons, dihalogen photoexcitation in Rg matrices continues to receive attention, as, for example, in ultrafast studies that directly probe the chemical processes occurring during the course of the reaction.[5]

Cryogenic parahydrogen (pH_2) matrices offer the same simplifying reaction conditions as Rg matrices for detailed photochemical studies.[6−10] In the case of dihalogen photoexcitation discussed here, the reaction dynamics should differ from the analogous reactions in Rg matrices due to the quantum mechanical nature of the pH_2 crystal. In quantum matrices such as solid pH_2, the kinetic energy of each pH_2 molecule associated with a lattice site is comparable to its potential energy, even at 0 K, and as a consequence, the zero-point excursions of the pH_2 molecules about the equilibrium lattice position is a substantial fraction (18%) of the nearest-neighbor spacing.[11,12] This combined with the low mass of the H_2 molecule suggests that the cage effect of the pH_2 solid should be minimal, and thus, excitation of a dihalogen above the dissociation threshold should lead to direct cage exit and permanent dissociation.[3] While the details of how effective the pH_2 matrix will be in dissipating energy along the dihalogen dissociation coordinate are not precisely known, the expectation is that due to the high thermal conductivity of solid pH_2 the excess energy should be rapidly dissipated.[8−10] These systems are less interesting from the standpoint of understanding photodissociation dynamics of solutes in conventional solvents, but rather how *in situ* photodissociation of dopants proceeds in quantum matrices both as a probe of the many-body pH_2 nuclear dynamics as well as how pH_2 matrices might be exploited to steer reaction dynamics in new ways to produce isolated highly reactive species.

Before detailed reaction dynamics studies are possible, however, the asymptotic photochemistry must be characterized. In comparison to Rg matrices, much less is known about the photochemistry of dihalogen molecules in pH_2 crystals. Momose and co-workers have pioneered photochemical studies[6] in solid pH_2 and have shown that alkyl halides readily photolyze at 260 nm to form alkyl radicals and iodine atoms in solid pH_2 and orthodeuterium (oD_2).[13,14] Work in this laboratory has demonstrated that Cl_2 can be efficiently photolyzed at 355 nm in pH_2, HD, and oD_2 crystals to produce permanently dissociated Cl atoms.[8−10] These studies are in stark contrast to analogous Br_2 photodissociation studies conducted in Rg matrices where permanent dissociation is suppressed even well above the dissociation threshold.[1,15,16]

The present study focuses on the 355 nm photodissociation of molecular bromine (Br_2) in solid pH_2 and oD_2. Excitation of Br_2 at 355 nm results in the dipole allowed electronic transition to the repulsive $C(^1\Pi_{1u})$ state well above the gas-phase dissociation threshold with approximately 6135 cm^{-1} of excess energy available to each atomic Br fragment.[17] Subsequent reaction of the nascent Br atom with the surrounding H_2 matrix is closed at these photodissociation energies due to the endothermicity of the $Br + H_2 \rightarrow HBr + H$ reaction (+6700 cm^{-1}).[18] Direct measurement of the Br atom photoproduction rate in pH_2 matrices is possible via the relatively weak electric-dipole forbidden Br spin−orbit (SO) transition ($^2P_{1/2}$←$^2P_{3/2}$) that can be detected under these conditions.[10,19] The relative Br_2 concentration can also be monitored through Br_2 induced hydrogen absorptions in the $Q_1(0)$ and $S_1(0)$ regions.[20−23]

* Electronic address: danderso@uwyo.edu.
† Present address: Department of Chemistry, University of Alberta, Edmonton, Alberta T6G 2G2, Canada.

10.1021/jp8029314 CCC: $40.75
Published on Web 10/09/2008

2. Experimental Section

We use the "rapid vapor deposition" technique of Fajardo and Tam to prepare millimeters-thick optically transparent crystals of Br_2 doped solid pH_2 and oD_2 suitable for Fourier transform infrared (FTIR) studies.[24,25] Details of the experimental setup and sample preparation technique have been reported elsewhere,[8−10] and here, we simply give a brief outline. Preparation of the 2−3 mm thick crystals involves codeposition of independent gas flows of Br_2 and pH_2 or oD_2 onto a precooled BaF_2 optical substrate within a sample-in-vacuum *l*He bath cryostat. In these experiments, 99.99% pH_2 and 97% oD_2 enriched solids are prepared by passing normal-H_2 or normal-D_2 gas through an ortho/para converter operated at, respectively, 14.5 and 18 K. The orthohydrogen (oH_2) concentration in the pH_2 crystals can be confirmed spectroscopically via the intensity of the oH_2 induced $Q_1(0)$ transition.[25] In the case of oD_2 samples, while the equilibrium concentration of oD_2 calculated at the 18 K temperature of the ortho/para converter is 98.8%, spectroscopic measurements reveal only 97% oD_2 enrichment.[26] For pH_2 crystals, sample thickness is determined from the integrated intensity of the $Q_1(0) + S_0(0)$ and $S_1(0) + S_0(0)$ double transitions.[27] The Br_2 concentration in these studies ranged from 25 to 90 parts per million (ppm) with the Br_2 gas delivered from the room-temperature vapor pressure of liquid bromine held in a glass tube and repeatedly frozen−pumped−thawed prior to use. On the basis of previous studies under similar conditions, the Br_2 molecules should be well-isolated, although this could not be confirmed spectroscopically. The Br_2 concentrations cited here are ratios of the quantities of Br_2 and H_2/D_2 entering the cryostat. These values may differ from the actual Br_2 concentrations in the solid but are estimated to be within ±40% of the *in situ* concentrations. As-deposited spectra were recorded at approximately 2 K right after deposition. Annealing the sample involves raising the temperature to 4.3 K for approximately 30 min.

The 355 nm output of a 10 Hz Nd:YAG laser (Spectra Physics Laboratory-170−10) with pulse energies adjusted from 2 to 5 mJ was used to generate Br atoms via *in situ* ultraviolet (UV) photodissociation of Br_2. Typically, the crystal was irradiated for 30−60 min right after deposition while maintaining the sample at 2 K. The unfocused 8 mm diameter UV laser beam impinged on the crystal at 45° with respect to the surface normal of the BaF_2 substrate. The IR beam is focused to approximately a 2 mm spot within the region irradiated by the UV laser to ensure that the entire region probed by the IR light has been UV-irradiated. For the photodissociation quantum yield measurements reported here, the as-deposited sample is irradiated for a specific amount of time and the UV pulse energy is measured with a power meter just outside the CaF_2 photolysis window on the vacuum shroud of the cryostat.

The infrared (IR) absorption spectra of Br atom doped solid pH_2 and oD_2 are recorded at resolutions ranging from 0.01 to 0.05 cm^{-1} (nominal with boxcar apodization) with a transmission experimental setup; the IR light propagates along the deposition surface normal. The FTIR spectrometer (Bruker IFS 120HR) was equipped in two different ways: (1) for near-IR studies (1900−9500 cm^{-1}), 100 scans with 0.05 cm^{-1} resolution were recorded with a tungsten source, CaF_2 beam splitter, and a liquid nitrogen cooled InSb detector; (2) for mid-IR studies (1800−5500 cm^{-1}), 49 scans with 0.01 cm^{-1} resolution were recorded with a globar source, KBr beam splitter, and a liquid nitrogen cooled InSb detector. The optical path outside the spectrometer and the cryostat was purged with dry N_2 gas to reduce atmospheric absorptions.

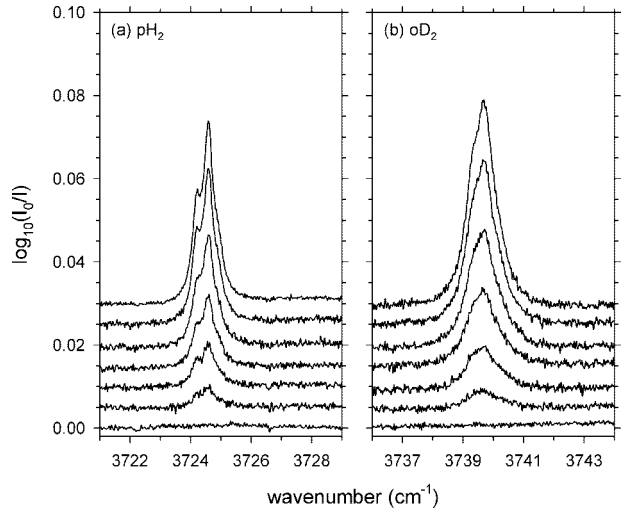

Figure 1. IR absorption spectra in the region of the zero-phonon Br SO transition for as-deposited Br_2 doped solid (a) pH_2 and (b) oD_2 as a function of exposure to the 355 nm photolysis laser. Traces are displaced upward with increasing UV exposure showing the photoproduction of isolated Br atoms. Photolysis conditions: (a) $[Br_2] = 70$ ppm, 2 mJ $pulse^{-1}$; (b) $[Br_2] = 60$ ppm, 2 mJ $pulse^{-1}$.

3. Results

3.1. Br_2 355 nm Photodissociation. Shown in Figure 1 are IR spectra in the region of the zero-phonon Br atom SO transition for Br_2 doped pH_2 and oD_2 crystals as a function of exposure to the 355 nm photolysis laser. The bottom traces in both spectra are before photolysis, showing no detectable absorption features in these two regions. Subsequent traces, displaced upward with increasing exposure to the UV photolysis laser, show the growth of the Br atom SO transition upon photolysis. In these as-deposited samples, the Br SO absorption feature appears as an unresolved doublet in solid pH_2 at 3724.2 and 3724.6 cm^{-1} and as an asymmetric peak at 3739.7 cm^{-1} in solid oD_2. The sharpness of the zero-phonon Br SO transition and the lack of a strong phonon sideband (not shown) indicate that the Br SO transition is in the weak electron−phonon coupling limit.[14] While also in the weak electron−phonon limit, halogen atom SO transitions in Rg matrices display stronger phonon sidebands.[19] The details of the Br SO line shapes in solid hydrogen will be discussed in a separate publication.[28]

Using the data shown in Figure 1, growth curves for the *in situ* photoproduction of Br atoms in solid pH_2 and oD_2 are plotted in Figure 2. The Br atom production rate is found to be approximately first-order. The quantum yield (Φ) for 355 nm photolysis of Br_2 is determined from the following first-order exponential growth expression[29]

$$I(t) = I_\infty(1 - \exp(-\sigma I_{355}\Phi t)) \quad (1)$$

where $I(t)$ and I_∞ are the integrated intensities of the Br SO transition at photolysis time t and at $t = \infty$, respectively, σ is the gas-phase cross section[17] of Br_2 at 355 nm (5.9×10^{-20} cm^2), and I_{355} is the laser flux (7.11×10^{16} photons s^{-1} cm^{-2}) used in the two experiments. The quantum yield for the 355 nm photolysis of Br_2 is $\Phi = 0.29(3)$ in solid pH_2 and $\Phi = 0.24(2)$ in oD_2. The reported errors are the uncertainty (1σ) in Φ determined from the least-squares fit of the data to eq 1. The magnitude of the effective quantum yield demonstrates that 355 nm photodissociation of Br_2 in either pH_2 or oD_2 is very efficient at producing isolated Br atoms. Photodissociation of Br_2 at 355 nm produces Br atoms with approximately 6135 cm^{-1} of translational energy per atom based on the dissociation energy[30]

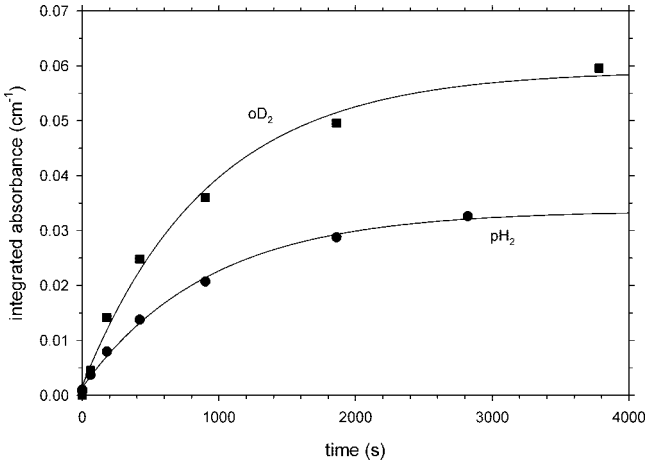

Figure 2. Plots of the Br SO transition integrated absorbance as a function of the time of 355 nm laser exposure for as-deposited solid pH_2 and oD_2. The data are generated from the spectra presented in Figure 1 and represented as filled circles (pH_2) and squares (oD_2). The solid lines are first-order kinetic fits to the data (see text for details).

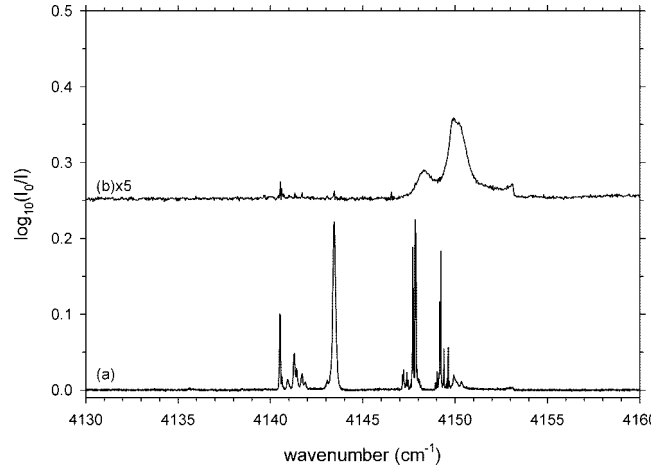

Figure 3. IR spectra in the $Q_1(0)$ induced region for a 40 ppm Br_2 doped pH_2 sample both (a) before and (b) after prolonged 355 nm photolysis. Note that the absorption intensity in trace (b) has been multiplied by a factor of 5 to facilitate comparison.

of Br_2 ($D_0 = 15\,900$ cm^{-1}) and the UV photon energy (28 169 cm^{-1}). Under these conditions, caging of the nascent photofragments by either quantum matrix is minimal. This is in stark contrast to Rg matrices where the cage effect dominates the Br_2 *in situ* photochemistry.[1,15,16]

As shown in Figure 2, the integrated intensity of the Br SO transition in oD_2 reaches a greater limiting value than in pH_2 even though the experimental conditions were quite similar (see Figure 1 caption for experimental conditions). These intensity differences are related at least in part to the absorption strength for the Br SO transition of Br trapped in solid pH_2 and oD_2. When Br is isolated in solid molecular hydrogen, the nearest-neighbor hydrogen molecules induce an electric dipole contribution to the Br SO transition moment, making the nominally forbidden transition stronger, and these induction effects can be different for solid pH_2 and oD_2. It is important to point out that the measured quantum yield using eq 1 is not sensitive to these intensity differences, but rather only to the rate (rate = $\sigma I_{355}\Phi$) at which Br atoms are photoproduced. The intensity differences for the SO transition of Br trapped in solid pH_2 and oD_2 will be discussed in a separate publication.[28]

3.2. Br_2 Induced pH_2 Transitions: $Q_1(0)$ and $S_1(0)$. To achieve better characterization of the Br atom doped pH_2 solids, which can be enriched to relatively high purities (e.g., 99.99% pH_2) via ortho/para conversion prior to deposition, the $Q_1(0)$ and $S_1(0)$ induced regions were examined.[20−22] These Br atom induced spectra can be compared to earlier studies of the analogous Rg atom doped pH_2 spectra to possibly identify signatures of the open-shell nature of the Br atom.[20,21] Interpretation of the spectra of Br atom doped oD_2 samples is complicated by overlapping absorptions induced by paradeuterium (pD_2), since the oD_2 samples can only be enriched to 97% levels using these techniques.

Representative spectra in the $Q_1(0)$ induced region (~4150 cm^{-1}) of a Br_2 doped pH_2 sample before and after photolysis are shown in Figure 3. For pure pH_2 solids, there are no absorptions in the $Q_1(0)$ region, and thus, all the peaks in Figure 3a are induced by the presence of impurities. Before photolysis, a number of relatively sharp features are observed from 4140 to 4151 cm^{-1} along with a strong, somewhat broader transition at 4143.5 cm^{-1}. Note that the asymmetric oH_2 induced $Q_1(0)$ feature due to residual oH_2 present in the sample is barely evident at 4153 cm^{-1}. After repeated photolysis and annealing cycles, the $Q_1(0)$ region transforms into two broad features at 4148.3 and 4149.9 cm^{-1}, with the higher-energy feature stronger in intensity. The comparatively sharp features observed prior to photolysis are assigned to Br_2 induced $Q_1(0)$ transitions; however, the details are still uncertain. The intensity of the broad peak at 4143.5 cm^{-1} displays a strong anticorrelation to the intensity of the Br SO peak upon photolysis, indicating that the intensity of this peak is a good measure of the relative Br_2 concentration. An analogous peak is observed in Br_2 doped oD_2 at 2978.83 cm^{-1}, which is similarly well isolated and has an intensity that tracks the Br_2 concentration.

The Br_2 molecule likely occupies a double substitution site and therefore does not rotate in the pH_2 crystal. As such, the environments of the surrounding pH_2 molecules differ, resulting in a number of sharp $Q_1(0)$ absorptions. As photolysis proceeds, all these features diminish in intensity, while the broad Br atom induced features increase. Accordingly, this region can be used to measure the extent of Br_2 photolysis. The spectrum shown in Figure 3 after photolysis represents one of the purest Br atom doped samples generated in this study due to the prolonged irradiation time for this particular crystal (2 h). The lack of any of the pre-photolysis absorptions in this region suggests the sample is completely photolyzed, and the Br_2 concentration is below some minimum value.

The fact that there are two broad features in the induced $Q_1(0)$ region after photolysis is interesting when this spectrum is compared to Rg atom doped solid pH_2 spectra. For Rg atom doped solid pH_2, the induced $Q_1(0)$ spectra consist only of a single feature, and the frequency and line shape of the peak signals how strongly localized the vibron excitation is around the Rg atom impurity.[20,31] For example, the Ar induced $Q_1(0)$ feature has a small shift to lower energy and is quite broad (2.0 cm^{-1}), indicating that the vibron is still effectively delocalized throughout the pH_2 crystal. While the Xe induced $Q_1(0)$ feature displays a larger shift and is quite sharp (0.11 cm^{-1}), consistent with a vibron strongly localized on pH_2 molecules adjacent to the Xe impurity.[20,31] For Kr, which is nearly isoelectronic with Br, the induced $Q_1(0)$ peak occurs at 4150.5 cm^{-1} with a fwhm of 1.1 cm^{-1}, which compares favorably to the more intense Br feature at 4149.9 cm^{-1} with a fwhm of 1.0 cm^{-1}. We speculate that the qualitatively different two-peak Br induced $Q_1(0)$ spectrum must in some way be related to the open-shell character of the Br atom.

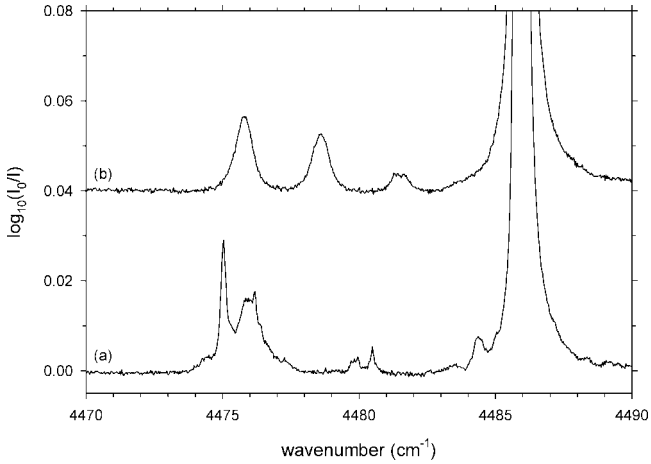

Figure 4. IR spectra in the $S_1(0)$ region (a) before and (b) after 355 nm photolysis for the same sample shown in Figure 3. The feature at 4486 cm^{-1} that goes off-scale is the $S_1(0)$ transition of pure solid pH_2.

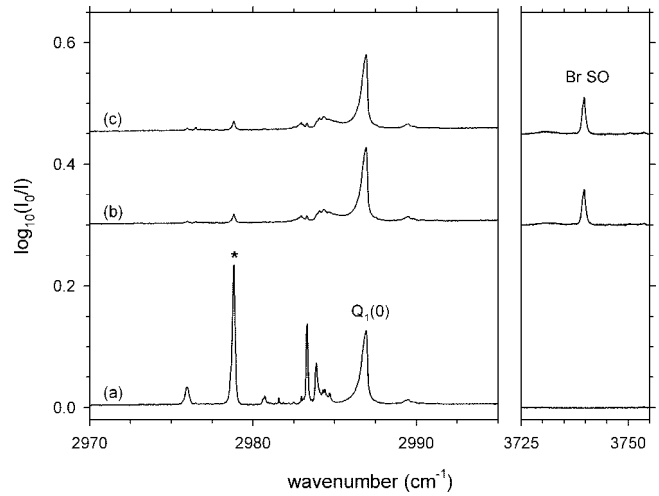

Figure 5. IR spectra in the $Q_1(0)$ region (2970−2995 cm^{-1}) and in the Br SO region (~3740 cm^{-1}) for a solid oD_2 sample doped with 60 ppm Br_2 at different steps in the *in situ* photoreaction. Trace (a) is the as-deposited sample before photolysis recorded at 2.11 K, trace (b) is recorded at 2.10 K after 127 min of 355 nm photolysis, and trace (c) is recorded at low temperature (2.07 K) after annealing the sample at 4.3 K for 30 min. The Br_2 induced $Q_1(0)$ feature at 2978.83 cm^{-1} is marked with an asterisk.

Similarly, spectra in the $S_1(0)$ region change as a function of the extent of photolysis of the Br_2 molecule. Spectra before and after photolysis are shown in Figure 4 in the $S_1(0)$ region for the same sample shown in Figure 3. Before photolysis, there are a number of features observed in this region. After photolysis, the spectrum simplifies to three relatively broad features at 4475.8, 4478.6, and 4481.5 cm^{-1}. This again is different from similar studies of the $S_1(0)$ region for Rg atom doped pH_2 solids.[21] In this case, the number of features is roughly consistent with the Rg atom studies, but the shift in the Br perturbed $S_1(0)$ transitions from the unperturbed value at 4485.97 cm^{-1} is much larger. For example, in the Rg atom studies[21] the largest observed shift was −3.83 cm^{-1} for Xe atoms, while for Br the largest shift is −10.1 cm^{-1}. This implies that the presence of the Br atom perturbs the $S_1(0)$ rovibron energy in solid pH_2 to a much greater extent than any of the Rg atoms studied. There are both isotropic and anisotropic contributions of the Br−H_2 intermolecular potential that can lead to the observed $S_1(0)$ shifts, but based on the Br induced $Q_1(0)$ results which only depend on the isotropic component, the large observed Br $S_1(0)$ shifts are likely due to greater anisotropic forces in the Br−H_2 intermolecular potential compared to Rg−H_2 intermolecular potentials.[32,33] Theoretical studies of the Br induced $Q_1(0)$ and $S_1(0)$ features are needed for more detailed analysis.

3.3. Infrared Detection of *in Situ* Br_2 Photolysis in Solid Hydrogen. One of the goals of this work is to develop the IR spectroscopic tools necessary to characterize the Br atom doped hydrogen solids created via *in situ* photolysis of Br_2 in order to utilize these materials to synthesize weakly bound halogen atom−molecule van der Waals complexes. By adding a codopant that does not photolyze at 355 nm, photolysis followed by gentle thermal annealing can be used to synthesize Br−molecule van der Waals complexes under low-temperature conditions. However, assignment of the resultant IR spectra of these complexes relies in part on being able to generate nearly pure Br atom doped samples with minimal amounts of unreacted Br_2. The induced $Q_1(0)$ region and Br SO transition allow both the photochemical reagents and products, respectively, to be monitored throughout the experiment.

Figure 5 illustrates how the extent of *in situ* Br_2 photolysis in solid oD_2 can be followed using IR spectroscopy. Spectra in the $Q_1(0)$ region (2987 cm^{-1}) for a solid oD_2 sample doped with 60 ppm of Br_2 are shown in Figure 5 at different steps of the *in situ* photoreaction. Trace (a) in Figure 5 is recorded at 2.1 K right after deposition. The sample in trace (a) thus contains only Br_2, and no absorption is detected in the Br SO region and a number of sharp Br_2 induced $Q_1(0)$ absorptions are observed from 2980 to 2990 cm^{-1}. The asymmetric absorption[26] at 2986.93 cm^{-1} in Figure 5 is the pD_2 induced $Q_1(0)$ absorption feature of pure solid oD_2. As discussed in section 3.2, the relative concentration of Br_2 can be deduced by the absorptions present in the induced $Q_1(0)$ region, particularly the absorption at 2978.83 cm^{-1} marked with an asterisk in Figure 5. Before photolysis, the Br_2 induced $Q_1(0)$ peaks are relatively intense as shown in trace (a) of Figure 5.

Trace (b) in Figure 5 is after 127 min of 10 Hz 355 nm photolysis at 2 mJ $pulse^{-1}$. The Br SO transition at 3739.7 cm^{-1} is now clearly visible, indicating the presence of Br atoms. Accordingly, the intensity of the Br_2 induced $Q_1(0)$ features decrease in intensity. Two broad Br atom induced $Q_1(0)$ features are visible just to the red of the pD_2 induced $Q_1(0)$ feature. However, even after greater than 2 h of photolysis there is still some unreacted Br_2 present as evidenced by the small Br_2 induced $Q_1(0)$ absorptions. Finally, in trace (c) the effect of thermal annealing on the spectrum is displayed. After thermal annealing, the intensity of the Br SO transition remains constant as well as the Br_2 induced $Q_1(0)$ feature at 2978.83 cm^{-1}. This indicates that annealing the sample at 4.3 K does not produce significant Br atom mobility in oD_2 to cause Br atom recombination. In contrast, annealing pH_2 solids doped with Br atoms at 4.3 K does produce measurable Br atom recombination. As a continuation of this work, we are studying weakly bound complexes of the Br atoms. Preliminary experiments have shown that Br−HBr complexes can be synthesized in this fashion and detected via IR absorptions of the complexed HBr molecule.[34]

4. Discussion

These studies demonstrate that *in situ* 355 nm photolysis of Br_2 can be effectively used to prepare relatively clean Br atom doped pH_2 and oD_2 crystals. The 355 nm photolysis wavelength used in this study is far to the blue of the Franck−Condon maximum (~420 nm) for transitions to the repulsive C-state,

TABLE 1: Spin−Orbit *k*-Values for Halogen Atoms in Hydrogen and Rg Matrices

halogen atom	oD_2	pH_2	Ar	Kr	Xe
Cl	1.080	1.069			
Br	1.0148	1.0106	1.0032	0.99388	0.98314
I	1.0068	1.0046	1.0019	0.99298	0.98073

and thus, it would be possible to study Br_2 photodissociation at lower photolysis energies closer to the dissociation threshold.[35,36] This makes the Br_2 system experimentally tractable for investigation of the caging ability of the hydrogen quantum solids as a function of photolysis energy over a broad range. Further, while the reaction $Br + H_2(v = 0) \rightarrow HBr + H$ is energetically closed at these photodissociation energies, the reaction $Br + H_2(v = 1) \rightarrow HBr + H$ is possible, since the reaction of Br with vibrationally excited H_2 is only 2540 cm^{-1} endoergic and may be overcome by the translational energy of the nascent Br photofragment. By irradiating solid pH_2 with IR radiation in the range 4100−4500 cm^{-1}, $H_2(v = 1)$ vibrons can be created in the solid.[8,9] These vibrons are highly mobile and have a lifetime on the order of microseconds, and thus can participate in the UV photoreaction. Coirradiation of the sample with IR and UV light may enable the HBr photoproduct to be produced. However, unlike analogous Cl_2 photodissociation studies where IR + UV coirradiation increases the HCl photoproduction rate significantly, no experiments have been conducted yet on IR + UV coirradiation of Br_2 doped samples. Further work aimed at trying to understand the details of Br_2 photodissociation in solid hydrogen matrices is underway.

Changes in SO splitting, both increases and decreases and even reversing of the energetic ordering, for atoms solvated in Rg matrices are well-documented in the literature.[37] The matrix host induced changes are interpreted in terms of the external heavy atom effect, which is the perturbation of the SO coupling in an atom due to a nearby atom of high atomic number. The mechanism governing the perturbation by the heavy atom, while not precisely known, is generally acknowledged to involve the SO enhanced admixture of singlet and triplet states.[37]

The IR absorption spectra presented here directly measure the SO splitting of Br isolated in solid pH_2 and oD_2, where we assume that the $^2P_{3/2}$ state is lower in energy than the $^2P_{1/2}$ state analogous to the gas phase. In Table 1, we summarize the SO measurements on halogen atoms (Cl, Br, and I) in both Rg and H_2 matrices by reporting $k = \Delta_{eff}/\Delta_{gas}$, defined as the ratio of the SO splitting of the halogen atom in a host and in the gas phase. As can be seen in Table 1, the *k*-values for Br steadily decrease going from Ar to Kr to Xe, but qualitatively change in going from Ar ($k > 1$) to Kr ($k < 1$). This subtle behavior is likely due to increasing heavy atom effects in going down the periodic table.

For halogen atoms isolated in solid hydrogen, a more appropriate way to think about the host-induced changes is that the SO states interact via different relativistic intermolecular potentials with the surrounding matrix molecules.[32,33,38] The effects of SO coupling on reshaping intermolecular potential energy surfaces is well-documented in small van der Waals clusters.[39] In this limit, the SO coupling remains that of the isolated halogen atom, but the two SO states ($^2P_{3/2}$ and $^2P_{1/2}$) interact with the pH_2 matrix via different intermolecular potentials. This leads to differing solvation energies of the two SO states, which are manifested in the shift of the SO transition energy from the gas-phase value. This point of view is more appropriate for solid hydrogen matrices compared to Rg matrices due to the small atomic number of hydrogen, i.e., there is no heavy atom effect in hydrogen matrices. In addition, the large-amplitude zero-point translational motion in the solid keeps the intermolecular distances near 3.8 Å where the SO coupling is not substantially affected.

In the ground $^2P_{3/2}$ state, the halogen atom unpaired Dirac electron cloud resembles a p-orbital, while in contrast in the excited $^2P_{1/2}$ state the Dirac electron cloud is isotropic and resembles an s-orbital. The halogen atom in the ground SO state possess an electric quadrupole moment and can interact with the H_2 host through quadrupole induced electrostatic terms, while in the $^2P_{1/2}$ state, the quadrupole moment is zero and these terms are absent.[39] Thus, the ground SO state ($^2P_{3/2}$) will, in general, experience a greater stabilization or solvation energy in solid pH_2 than the excited SO state ($^2P_{1/2}$), and the measured SO transition energy will shift to higher energy. The observed *k*-values for all three halogen atoms in solid pH_2 and oD_2 are consistent with this simple picture; the *k*-values are always greater than 1. Comparison of the halogen atom *k*-values in solid hydrogen and Rg matrices suggests that heavy atom effects are significant in Kr and Xe, but less important in Ar, as expected from chemical intuition.

The halogen atom SO shifts in the two isotopomers of hydrogen studied are also measurably different, which cannot arise within the Born−Oppenheimer approximation from pure electronic effects, such as the heavy atom effect. For all three halogen atoms investigated, the *k*-value in oD_2 is consistently greater than in solid pH_2. This difference likely results from zero-point averaging over the intermolecular interactions in the two solids. In quantum solids, the amount of translational zero-point motion is reflected by the nearest-neighbor spacing. In pH_2, the nearest neighbor spacing is 3.789 Å, while in oD_2, it is 3.605 Å.[11] The reduced zero-point motion in oD_2 results in an effectively smaller solvent cage for the halogen atom, and thus, a larger perturbation is observed.

Another significant difference between the pH_2 and oD_2 solids is the approximately 300 times larger $J = 1$ concentration in samples of oD_2 compared to pH_2. It is well-known that in general the attractive interactions of a dopant species with a $J = 1$ hydrogen species are greater than a $J = 0$ species, because the $J = 1$ hydrogen molecule can interact with the dopant through both anisotropic and isotropic intermolecular forces, while for the $J = 0$ hydrogen species, all anisotropic interactions average to zero.[8,40,41] Previous measurements have demonstrated that these differences in the intermolecular forces of the dopant with $J = 1$ and $J = 0$ hydrogen species can lead to clustering of the $J = 1$ species to the dopant in hydrogen matrices. Furthermore, $J = 1$ clustering to the dopant can induce measurable shifts in the dopant IR spectrum. However, in this case $J = 1$ clustering to Br atoms is not thought to be responsible for the observed shift in the SO transition of Br trapped in oD_2 and pH_2, because open-shell paramagnetic species dramatically enhance nuclear spin conversion between ortho and para states.[42,43] Specifically, any $J = 1$ species that clusters to a Br atom in a solid hydrogen matrix should be rapidly (on the time scale of FTIR measurements) converted to a $J = 0$ species. Previous unpublished results from this laboratory for Cl atoms in 97% pure pH_2 matrices support this interpretation; that is, the frequency and line shape of the Cl SO transition is the same in both 97% and 99.99% pure pH_2 after an hour.

The last observed trend is that the perturbation of the halogen atom SO splitting increases for halogen atoms higher on the periodic table. The largest *k*-value is observed for Cl and the *k*-value closest to 1.00 is observed for I atoms. This trend suggests that for Cl, which has the smallest SO splitting of the

halogen atoms studied, the difference in the solvation energies of the two Cl SO states is most pronounced. While the behavior contained in this trend ultimately reflects differences in the shapes of the halogen atom$-H_2$ relativistic intermolecular potentials, the experimental observable involves many-body effects, large amplitude translational zero-point averaging, multiple potential energy surfaces, and potentially nonadiabatic processes in the presence of SO coupling.

5. Conclusion

These IR spectroscopic studies demonstrate that 355 nm *in situ* photolysis of Br_2 precursor molecules is an effective and clean way to generate Br atom doped pH_2 and oD_2 solids. Under these conditions, the Br atom photoproduction rate is found to be approximately first-order, allowing an effective quantum yield of $\Phi = 0.29(3)$ in pH_2 and $\Phi = 0.24(2)$ in oD_2 to be measured. Such relatively high quantum yields are in stark contrast to analogous photochemical studies in Rg matrices where caging of the nascent photofragments dominates the photochemistry. It thus would be interesting to conduct photochemical studies of Br_2 in quantum matrices of solid hydrogen at lower photodissociation energies to determine where and if caging becomes important and if access to excited Br_2 bound states results in detectable fluorescence signals.

The direct observation of the Br SO transition provides a spectroscopic signature of how the two fine structure states of Br interact differently with the surrounding host molecules. The present measurements when combined with literature values suggest that the changes in the measured SO splitting for Br atoms in solid hydrogen matrices represent solely different solvation energies for the two Br SO states, which can be compared with *ab initio* predictions of the Br$-H_2$ intermolecular potential including relativistic effects. However, this comparison is not straightforward, since the measurements reflect both nuclear dynamics on the potential energy surfaces and many-body contributions to the electronic surfaces. Halogen atoms in solid hydrogen matrices nonetheless represent benchmark systems where a fully molecular level understanding of radicals and radical reactions in a condensed phase may first be realized.

Acknowledgment. This research was supported by the U.S. National Science Foundation (CHE-0316268). The authors would like to thank Heide N. Ibrahim for helpful discussions about her ultrafast studies of the valence transitions of Br_2 in Ar matrices.

References and Notes

(1) Mandich, M.; Beeken, P.; Flynn, G. *J. Chem. Phys.* **1982**, *77*, 702.
(2) McCaffrey, J. G.; Kunz, H.; Schwentner, N. *J. Chem. Phys.* **1992**, *96*, 155.
(3) Apkarian, V. A.; Schwentner, N. *Chem. Rev.* **1999**, *99*, 1481.
(4) Rabinowitch, E.; Wood, R. C. *Trans. Faraday Soc.* **1936**, *32*, 1381.
(5) Guhr, M.; Bargheer, M.; Fushitani, M.; Kiljunen, T.; Schwentner, N. *Phys. Chem. Chem. Phys.* **2007**, *9*.
(6) Momose, T.; Shida, T. *Bull. Chem. Soc. Jpn.* **1998**, *71*, 1.
(7) Momose, T.; Fushitani, M.; Hoshina, H. *Int. Rev. Phys. Chem.* **2005**, *24*, 533.
(8) Yoshioka, K.; Raston, P. L.; Anderson, D. T. *Int. Rev. Phys. Chem.* **2006**, *25*, 469.
(9) Raston, P. L.; Anderson, D. T. *Phys. Chem. Chem. Phys.* **2006**, *8*, 3124.
(10) Raston, P. L.; Anderson, D. T. *J. Chem. Phys.* **2007**, *126*, 021106.
(11) Silvera, I. F. *Rev. Mod. Phys.* **1980**, *52*, 393.
(12) Van Kranendonk, J. *Solid Hydrogen - Theory of the Properties of Solid H_2, HD, and D_2*; Plenum Press: New York, 1983.
(13) Fushitani, M.; Momose, T.; Shida, T. *Chem. Phys. Lett.* **2002**, *356*, 375.
(14) Fushitani, M.; Miyamoto, Y.; Hoshina, H.; Momose, T. *J. Phys. Chem. A* **2007**, *111*, 12629.
(15) Ault, B. S.; Howard, W. F.; Andrews, L. *J. Mol. Spectrosc.* **1975**, *55*, 217.
(16) Ibrahim, H. (private communication).
(17) Hubinger, S.; Nee, J. B. *J. Photochem. Photobiol., A* **1995**, *86*, 1.
(18) Huber, K. P.; Herzberg, G. *Constants of Diatomic Molecules*; Van Nostrand: New York, 1979.
(19) Pettersson, M.; Nieminen, J. *Chem. Phys. Lett.* **1998**, *283*, 1.
(20) Raston, P. L.; Anderson, D. T. *Low Temp. Phys.* **2007**, *33*, 653.
(21) Raston, P. L.; Anderson, D. T. *J. Mol. Spectrosc.* **2007**, *244*, 128.
(22) Anderson, D. T.; Hinde, R. J.; Tam, S.; Fajardo, M. E. *J. Chem. Phys.* **2002**, *116*, 594.
(23) Hinde, R. J.; Anderson, D. T.; Tam, S.; Fajardo, M. E. *Chem. Phys. Lett.* **2002**, *356*, 355.
(24) Fajardo, M. E.; Tam, S. *J. Chem. Phys.* **1998**, *108*, 4237.
(25) Tam, S.; Fajardo, M. E. *Rev. Sci. Instrum.* **1999**, *70*, 1926.
(26) Crane, A.; Gush, H. P. *Can. J. Phys* **1966**, *44*, 373.
(27) Tam, S.; Fajardo, M. E. *Appl. Spectrosc.* **2001**, *55*, 1634.
(28) Raston, P. L.; Kettwich, S. C.; Anderson, D. T. (in preparation).
(29) Eloranta, J.; Vaskonen, K.; Hakkanen, H.; Kiljunen, T.; Kunttu, H. *J. Chem. Phys.* **1998**, *109*, 7784.
(30) Jee, Y.-J.; Jung, Y.-J.; Jung, K.-H. *J. Chem. Phys.* **2001**, *115*, 9739.
(31) Hinde, R. J. *J. Chem. Phys.* **2003**, *119*, 6.
(32) Klos, J.; Chalasinski, G.; Szczesniak, M. M. *J. Phys. Chem. A* **2002**, *106*, 7362.
(33) Klos, J.; Szczesniak, M. M.; Chalasinski, G. *Int. Rev. Phys. Chem.* **2004**, *23*, 541.
(34) Kettwich, S. C.; Pinelo, L. F.; Anderson, D. T. *Phys. Chem. Chem. Phys.* **2008**, *10*, 5477.
(35) Passchier, A. A.; Christian, J. D.; Gregory, N. W. *J. Phys. Chem.* **1967**, *71*, 937.
(36) Asano, Y.; Yabushita, S. *Chem. Phys. Lett.* **2003**, *372*, 348.
(37) Pellow, R.; Vala, M. *J. Chem. Phys.* **1989**, *90*, 5612.
(38) Kurosaki, Y.; Takayanagi, T. *J. Chem. Phys.* **2003**, *119*, 7838.
(39) Dubernet, M.-L.; Hutson, J. M. *J. Phys. Chem.* **1994**, *98*, 5844.
(40) Yoshioka, K.; Anderson, D. T. *J. Chem. Phys.* **2003**, *119*, 4731.
(41) Yoshioka, K.; Anderson, D. T. *J. Mol. Struct.* **2006**, *786*, 123.
(42) Shevtsov, V.; Milmi, P.; Ylinen, E.; Punkkinen, M. *Physica B* **2000**, *284−288*, 385.
(43) Abouaf-Marguin, L.; Vasserot, A.-M.; Pardanaud, C.; Stienlet, J.; Michaut, X. *Chem. Phys. Lett.* **2008**, *454*, 61.

JP8029314